Electronic Raman scattering of $s+g$-wave superconductors: Implications for borocarbide superconductors

Hyun C. Lee* and Han-Yong Choi
BK21 Physics Research Division and Institute of Basic Science, Department of Physics, Sung Kyun Kwan University, Suwon 440-746, Korea

(Received 23 October 2001; revised manuscript received 28 February 2002; published 7 May 2002)

The electronic Raman scattering of borocarbide superconductors is studied based on the weak-coupling theory with $s+g$-wave gap symmetry. The low-energy behaviors and the relative peak positions can be naturally understood, while the explanation of the detailed shape of the B_{1g} peak seems to require a strong inelastic interaction not present in the weak-coupling theory.

DOI: 10.1103/PhysRevB.65.174530 PACS number(s): 74.70.Dd, 74.20.Rp, 78.30.−j

I. INTRODUCTION

Electronic Raman scattering is a very useful probe in determining the symmetry of the order parameter of superconductors (SC's).[1] It plays an especially important role in the study of unconventional superconductors owing to the strong dependence of Raman responses on the symmetry of superconducting order parameters. Along with the discovery of high-temperature superconductors, other unconventional superconductors have been actively investigated, for example, Borocarbide superconductors (BCSC)[2] (Y,Lu)Ni_2B_2C, and ruthenate superconductors[3] Sr_2RuO_4. The symmetry of the order parameter of high-temperature SC's and Ruthenate SC's is believed to be d wave[4] and p wave,[3] respectively. However, the symmetry of the order parameter of BCSC has not been determined unambiguously at present. Nevertheless, there is growing experimental evidence of the strongly anisotropic nature of order paramter of BCSC. Band-structure calculations[5,6] and a T_c versus γ plot[7] suggest strong electron-phonon interaction as a possible origin of BCSC. In general, the superconductivity mediated by electron-phonon interaction has an isotropic s-wave superconducting gap (SG), and the nodes of the gap on the Fermi surface (FS) do not exist.

On the other hand, the following experiments indicate the existence of the nodes of a SG: (1) the power-law temperature dependence (T^3) of the nuclear relaxation rate[8] $1/T_1$ suggests the existence of line nodes of the superconducting gap on the Fermi surface.[9] Moreover, a Hebel-Slichter peak is not observed,[8] which is also consistent with the existence of nodes. (2) The magnetic-field (H) dependence of the residual density of states in the vortex state[10,11] was observed to be $\sqrt{H}$. According to the well-known result by Volovik,[12] $\sqrt{H}$ indicates the existence of lines of gap nodes on the FS. (3) Metlushko *et al.* reported an observation of the fourfold symmetric upper critical field.[13] Evidently, such a behavior is not compatible with the isotropic s-wave gap, and has been interpreted in terms of *three*-dimensional d-wave superconductivity.[14] (4) A *direct* measurement of the SG by photoemission spectroscopy[15] also demonstrates the existence of nodes of the SG. (5) A recent experiment by Boaknin *et al.* on the thermal conductivity of $LuNi_2B_2C$ showed that the magnetic-field dependence of thermal conductivity at low temperature is very similar to that of a heavy-fermion SC with a gap which has *lines of nodes*.[16]

Experimental facts (1)–(5) clearly corroborate a gapless superconductivity, the simplest of which is d-wave superconductivity. However, the following experiments for BCSC with Ni substituted by some impurity element as Pt pose serious challenges for the d-wave scenario: (6) The magnetic field H dependence of residual density of states in the vortex state[10,11] changes from $\sqrt{H}$ to H upon the impurity substitution. Caroli *et al.*[17] showed that the H dependence is linear for an isotropic s-wave SC. (7) The detailed plot of $\ln[C(T)/\gamma T_c]$ versus T_c/T also demonstrates the change of behavior from T^3 to the activated one.[18] (8) The photoemission experiment shows the opening of gap over the whole FS for impurity substituted compound by comparing the shapes of the spectra of pure and dirty BCSC.

The experiments for the dirty BCSC [(6)–(8)] implied that the gap symmetry cannot be a simple d wave because the introduction of impurities does not change the gap anisotropy owing to the d-wave symmetry,[19] and only overall amplitudes decrease with the impurity concentrations. In connection with the experiments for the diry BCSC, we note that the superconducting temperature of a conventional s-wave SC is insensitive to the introduction of nonmagnetic impurities, which is the fact known as Anderson theorem,[20] while unconventional SC's depend on them sensitively.[19,21] Finally there is no experimental evidence of broken tetragonal symmetry, thus we are forced to rule out pairing interactions which violate tetragonal symmetry.

Synthesizing all of the above observations, (1)–(5) and (6)–(8), and the unbroken tetragonal symmetry, we are led to a proposal that the gap symmetry of BCSC should be a mixed one which respects the tetragonal symmetry. Obviously, the simplest possible candidate is the $(s+g)$-wave gap symmetry. The gap function of the form $\Delta(\phi) = |\Delta_0 \cos(2\phi)|$ is also a viable choice, but nodes of gaps of this kind are accidental and are not enforced by symmetry. From the symmetry viewpoint, an $s+g$-wave gap is more natural. We note that Maki *et al.* also adopted the model of BCSC with the $(s+g)$-wave gap symmetry in their recent preprint.[22]

Yang *et al.* studied[23] BCSC by means of electronic Raman scattering. They observed 2Δ-like peaks in A_{1g}, B_{1g},

and B_{2g} geometries. The peak position of B_{1g} geometry is found to be larger than the others. Also, peaks of A_{1g} and B_{2g} symmetries are much stronger than the peak of B_{1g} symmetry. There exists a scattering strength below the 2Δ gap, which increases with frequency *linearly* in B_{1g} and B_{2g} geometries (see Fig. 5).

We intend to understand the qualitative features of the above Raman experiments based on the simplest model with $s+g$-wave gap symmetry. We adopt the weak-coupling theory with a separable pairing interaction. Then, even if the physical origin of the pairing interaction is unknown, we can deduce many physical consequences which depend mainly on the pairing symmetry and not on the details of interactions. Strictly speaking, the weak-coupling theory is not expected to be valid on a quantitative level, and indeed the band theory calculation predicts the electron-phonon interaction to lie in the strong-coupling regime. Nevertheless, we believe that the qualititave features might be understood with the simple weak-coupling model.

We find that the relative peak positions and the nature of scattering strengh below the 2Δ gap can be understood naturally, while the weak and broad B_{1g} peak features cannot be explained in a simple weak-coupling theory with $s+g$-wave gap symmetry. Presumably, in a B_{1g} geometry, other inelastic-scattering mechanisms in the particle-hole channel become important. The B_{1g} phonon may provide one such scattering mechanism.

This paper is organized as follows: In Sec. II, we briefly summarize basic formalisms of electronic Raman scattering. In Sec. III, explict expressions for the Raman intensity of a $s+g$-wave SC are derived. The physical results are presented in Sec. IV, and we conclude this paper with a summary and discussion in Sec. V.

II. FORMALISM

The general formalisms for the electronic Raman scattering of superconductors are well expounded upon in papers by Klein and Dieker,[24] Monien and Zawadowski,[25] and Devereaux and Einzel.[26] Here we shall briefly summarize the main results of the above papers necessary for our discussions.

The electronic Raman cross section is proportional to the dynamical structure factor $S(\omega,\mathbf{q})$,

$$S(\omega,\mathbf{q})=[1+n_B(\omega)]\left[-\frac{1}{\pi}\mathrm{Im}\chi^R_{\tilde{\rho}\tilde{\rho}}(\omega,\mathbf{q})\right], \tag{1}$$

where $n_B(\omega)$ is the Bose distribution function and the superscript R of $\chi^R_{\tilde{\rho}\tilde{\rho}}$ denotes the retarded correlation function. The effective density-density correlation function $\chi_{\tilde{\rho}\tilde{\rho}}$ (in imaginary time) is defined by

$$\chi_{\tilde{\rho}\tilde{\rho}}(\tau-\tau',\mathbf{q})=-\langle T_\tau\tilde{\rho}_\mathbf{q}(\tau)\tilde{\rho}_{-\mathbf{q}}(\tau')\rangle. \tag{2}$$

$\tilde{\rho}_\mathbf{q}$ is the effective density operator,

$$\tilde{\rho}_\mathbf{q}=\sum_{\mathbf{p},\sigma}\gamma_\mathbf{p}c^\dagger_{\mathbf{p}+\mathbf{q}/2,\sigma}c_{\mathbf{p}-\mathbf{q}/2,\sigma}. \tag{3}$$

For nonresonant electronic Raman scatterings, the coefficient $\gamma_\mathbf{p}$ is given by

$$\gamma_\mathbf{p}=\sum_{\alpha\beta}e^I_\alpha\frac{\partial^2\epsilon_\mathbf{p}}{\partial p_\alpha\partial p_\beta}e^F_\beta, \tag{4}$$

where e^I and e^F are the polarization vectors of the incoming and outgoing photons, respectively. $\epsilon_\mathbf{p}$ is the energy dispersion of material. α and β label the coordinates perpendicular to the photon momentum.

Light couples with the charge fluctuations in the material, and in this case the long-range Coulomb interaction should be summed in the random phase approximation (RPA). The RPA summation implements the screening effect. Let us define *irreducible* correlation functions which do *not* include the RPA-type diagrams as subdiagrams

$$\pi_{\gamma\gamma}(\mathbf{q},\tau-\tau')=-\langle T_\tau\tilde{\rho}_\mathbf{q}(\tau)\tilde{\rho}_{-\mathbf{q}}(\tau')\rangle_{\mathrm{irr}}, \tag{5}$$

$$\pi_{\gamma 0}(\mathbf{q},\tau-\tau')=-\langle T_\tau\tilde{\rho}_\mathbf{q}(\tau)\rho_{-\mathbf{q}}(\tau')\rangle_{\mathrm{irr}}, \tag{6}$$

$$\pi_{0\gamma}(\mathbf{q},\tau-\tau')=-\langle T_\tau\rho_\mathbf{q}(\tau)\tilde{\rho}_{-\mathbf{q}}(\tau')\rangle_{\mathrm{irr}}, \tag{7}$$

$$\pi_{00}(\mathbf{q},\tau-\tau')=-\langle T_\tau\rho_\mathbf{q}(\tau)\rho_{-\mathbf{q}}(\tau')\rangle_{\mathrm{irr}}, \tag{8}$$

where $\rho_\mathbf{q}=\Sigma_{\mathbf{p},\sigma}1\ c^\dagger_{\mathbf{p}+\mathbf{q}/2,\sigma}c_{\mathbf{p}-\mathbf{q}/2,\sigma}$ is an ordinary density operator. Then the correlation function $\chi_{\tilde{\rho}\tilde{\rho}}$ can be written as

$$\chi_{\tilde{\rho}\tilde{\rho}}=\left[\pi_{\gamma\gamma}-\frac{\pi_{\gamma 0}\pi_{0\gamma}}{\pi_{00}}\right]+\frac{\pi_{\gamma 0}\pi_{0\gamma}}{\pi^2_{00}}\chi_{\rho\rho}, \tag{9}$$

where $\chi_{\rho\rho}$ is the density-density correlation function which is negligible in the low $\mathbf{q}$ limit. In the low $\mathbf{q}$ limit, only the first term in the brackets of Eq. (9) needs to be considered.

$$\lim_{\mathbf{q}\to 0}\chi_{\tilde{\rho}\tilde{\rho}}(i\omega,\mathbf{q})=\pi_{\gamma\gamma}(i\omega,\mathbf{q})-\frac{\pi_{\gamma 0}(i\omega,\mathbf{q})\pi_{0\gamma}(i\omega,\mathbf{q})}{\pi_{00}(i\omega,\mathbf{q})}. \tag{10}$$

The second term on the right-hand side of Eq. (10) is usually referred to as the screening correction.

The vertex factor $\gamma_\mathbf{p}$ for the lattice with tetragonal symmetry in various scattering geometries are given by

$$\gamma_{A_{1g}}(\phi)=1+\gamma_A\cos 4\phi,$$

$$\gamma_{B_{1g}}(\phi)=\gamma_{B_1}\cos 2\phi,$$

$$\gamma_{B_{2g}}(\phi)=\gamma_{B_2}\sin 2\phi. \tag{11}$$

There can be terms with higher harmonics such as $\cos(4N\phi)$, $\cos[(4N-2)\phi]$, and $\sin[(4N-2)\phi]$ with $N\geq 2$ in Eq. (11). We will ignore them, but in the detailed fitting of experimental data, the higher harmonics terms are necesary.[26] The factor 1 for the A_{1g} geometry case of Eq. (11) is canceled by the screening correction; therefore, effectively, $\gamma_{A_{1g}}(\phi)\to\gamma_A\cos 4\phi$.

The coefficients γ_A, γ_{B_1}, and γ_{B_2} are determined by the shape of the energy band. If we take a simple band structure with tetragonal symmetry (a is a lattice constant),

$$\epsilon_{\mathbf{p}} = -2t[\cos(p_x a)+\cos(p_y a)] + 4t'\cos(p_x a)\cos(p_y a) - 2t_z\cos(p_z a), \tag{12}$$

then $\gamma_{B_{1g}} \propto t$, $\gamma_{B_{2g}} \propto t'$ and $\gamma_A \propto \text{const}\times t + \text{const}\times t'$. From the average Fermi velocities[5] we can estimate $t \sim 0.2$ eV and $t' \sim 0.1$ eV. In our work, we will simply put $\gamma_A = \gamma_{B_1} = \gamma_{B_2} = 1$. Thus there are some reservations in comparing the relative intensities of theoretical results with those of experimental ones.

III. $s+g$-WAVE SUPERCONDUCTOR

The gap function of the $s+g$-wave superconductor is

$$\Delta(\phi) = \Delta_s + \Delta_g\cos(4\phi), \quad 0 < \Delta_s < \Delta_g, \tag{13}$$

where ϕ is the azimuthal angle in spherical polar coordinate. The weak dependence on the radial momentum is neglected ($k = k_F$). Since the amplitude of the g-wave part is larger than the s-wave part, the *lines* of nodes exist on the FS. In the opposite case $\Delta_s > \Delta_g$ the gap function does not have nodes, and it behaves like a gapful anisotropic s-wave SC. The cases $0 < \Delta_s < \Delta_g$ and $0 < \Delta_g < \Delta_s$ are physically relevant for pure BCSC and dirty BCSC, respectively. We will use the Nambu formalism for the computation of correlation functions in a superconducting state. The one-particle Green function in the weak-coupling approximation is given by

$$\hat{G}(i\epsilon, \mathbf{p}) = \frac{i\epsilon\tau_0 + \xi_{\mathbf{p}}\tau_3 + \Delta_{\mathbf{p}}\tau_1}{(i\epsilon)^2 - \xi_{\mathbf{p}}^2 - \Delta_{\mathbf{p}}^2}, \tag{14}$$

where τ_i's are the Pauli matrices in Nambu space. The wave-function renormalization $Z(i\epsilon)$ is neglected, and the frequency dependence of interaction is encoded in the cutoff ω_c [see Eq. (18)] of the pairing potential in momentum space. In Nambu notation, the correlation functions $\pi_{\gamma\gamma'}$ can be expressed as $[p = (i\epsilon, \mathbf{p}), q = (i\omega, \mathbf{q})]$

$$\pi_{\Gamma\gamma'}(q) = \frac{T}{N}\sum_p \mathrm{Tr}[\hat{\Gamma}_{p,p+q}\hat{G}(p)\hat{\gamma'}_{\mathbf{p}+\mathbf{q}}\hat{G}(p+q)], \tag{15}$$

where N is the number of lattice sites. $\hat{\Gamma}_{p,p+q}$ is the renormalized vertex function. We will evaluate the vertex function in the ladder approximation. The unrenormalized (bare) vertex function is

$$\hat{\Gamma}_{p,p+q} = \hat{\gamma}_{\mathbf{p}} = \tau_3\gamma_{\mathbf{p}}. \tag{16}$$

The gap equation of the (spin-singlet) $s+g$-wave SC reads

$$\Delta(\phi) = -\frac{1}{N}\sum_{\mathbf{p}'} D_{\mathbf{p}\mathbf{p}'}\frac{\tanh(E_{\mathbf{p}'}/2T)}{2E_{\mathbf{p}'}}\Delta(\phi'), \tag{17}$$

where $D_{\mathbf{p}\mathbf{p}'}$ is the pairing potential in momentum space, and $E_{\mathbf{p}'} = \sqrt{\xi_{\mathbf{p}'}^2 + \Delta_{\mathbf{p}'}^2}$.

The gap equation [Eq. (17)] can be solved in a closed form for separable pairing interactions. Given the specific form of the gap [Eq. (13)], the separable pairing interaction which respects the tetragonal symmetry should be chosen as

$$D_{\mathbf{p}\mathbf{p}'} = [D_s + D_g\cos 4\phi\cos 4\phi' + D_{sg}(\cos 4\phi + \cos 4\phi')] \times \Theta(\omega_c - |\xi_{\mathbf{p}}|)\Theta(\omega_c - |\xi_{\mathbf{p}'}|), \tag{18}$$

where $\Theta(x)$ is the step function. The numerical values of the coupling constants D_s, D_{sg}, and D_g are determined to be consistent with the values of Δ_s and Δ_g, and the superconducting transition temperature T_c. For details, see Appendix C. Since there is no dependence on the polar angle θ in Eq. (15), the momentum integration can be written as

$$\frac{1}{N}\sum_{\mathbf{p}} = N_F\int d\xi_{\mathbf{p}}\frac{1}{2\pi}\int_0^{2\pi} d\phi, \tag{19}$$

where N_F is the density of states per spin. Note that the spin sum is implicit in the trace over Nambu space. For later references, let us define the dimensionless coupling constants.

$$\lambda_s = -N_F D_s, \quad \lambda_g = -N_F D_g, \quad \lambda_{sg} = -N_F D_{sg}. \tag{20}$$

The technical analysis of Eq. (15) crucially depends on whether a bare or renormalized vertex is used.

A. Analysis for the bare vertex

Henceforth we will consider only the zero-temperature case for simplicity. For the bare vertex, the integrals over frequency and $|\mathbf{p}|$ of Eq. (15) can be done explicitly. Then the imaginary parts of $\pi^R_{\gamma\gamma'}$ can be expressed as a single integral over an azimuthal angle ϕ:

$$-\mathrm{Im}\,\pi^R_{\gamma\gamma'} = \frac{4N_F}{\omega}\mathrm{Re}\left[\int_0^{2\pi}\frac{d\phi}{2\pi}\frac{\gamma(\phi)\gamma'(\phi)\Delta^2(\phi)}{\sqrt{\omega^2 - 4\Delta^2(\phi)}}\right]. \tag{21}$$

At finite temperature the factor $\tanh(\omega/4T)$ should be multiplied by the above result.

At this point we note that the screening correction is absent for B_{1g} and B_{2g} symmetries. The screening correction can re-expressed as

$$\pi_{\gamma 0} = N_F\int_0^{2\pi}\frac{d\phi}{2\pi}[\gamma(\phi)\times 1]\Delta^2(\phi)f(\cos 4\phi), \tag{22}$$

where f is a certain complex function which can be expanded in a power series with respect to the argument. Clearly the integrals of Eq. (22) vanish for the vertex $\gamma(\phi) = \cos 2\phi$ or $\gamma(\phi) = \sin 2\phi$, since they are orthogonal to $\cos 4N\phi$ with $N \geqslant 1$. Thus the screening corrections for B_{1g} and B_{2g} symmetries vanish. The A_{1g} vertex $\cos(4\phi)$ has a finite overlap with the rest of integrand, and there is nonzero screening correction for A_{1g} symmetry. The integral equation (21) cannot be done in a closed form, and the numerical integrations are required. The results are presented in Sec. IV A.

B. Analysis for the renormalized vertex

The vertex correction will be evaluated within the ladder approximation. We will include the corrections coming from the pairing interaction only. In principle, other interactions may well contribute to the vertex correction. However, we do not have enough experimental informations to identify the specific interactions responsible for scatterings in particle-hole channel. Evidently this approximation should be improved, and in fact, from the comparison with the Raman experiment we expect the existence of strong inelastic scatterings with B_{1g} symmetry in the particle-hole channel. Here we choose to work in the simplest approximation of including the pairing interaction only.

The summation of ladder diagrams is equivalent to solving an integral equation of the following type:

$$\hat{\Gamma}_\gamma(\mathbf{p}+\mathbf{q}/2,\mathbf{p}-\mathbf{q}/2,i\omega) = \hat{\gamma}(\mathbf{p}+\mathbf{q}/2,\mathbf{p}-\mathbf{q}/2)+\frac{T}{N}\sum_{i\epsilon',\mathbf{p}'}[(-1)D_{\mathbf{pp}'}] \times\tau_3\hat{G}(\mathbf{p}'-\mathbf{q}/2,i\epsilon')\hat{\Gamma}_\gamma\left(\mathbf{p}'+\frac{\mathbf{q}}{2},\mathbf{p}'-\frac{\mathbf{q}}{2},i\omega\right) \times\hat{G}\left(\mathbf{p}'+\frac{\mathbf{q}}{2},i\epsilon'+i\omega\right)\tau_3. \quad (23)$$

The retardation effect in the weak-coupling approximation is reflected in the cutoff of the pairing interaction in *momentum space*, then the frequency channel can be treated as instantaneous. For such an interaction, the vertex correction $\hat{\Gamma}$ becomes independent of the incoming frequency $i\epsilon$, which is an extremely crucial simplification. In fact, for a fully self-consistent treatment, the renormalized Green function $\hat{G}$ with $[Z(i\epsilon)\neq 1]$ should be used, which incoporate the self-energy correction due to scatterings in the particle-hole channel. However, if the underlying system is a Fermi liquid, the $Z(i\epsilon)$ correction is not expected to introduce qualitative changes.

The momentum transfer $\mathbf{q}$ can be neglected for a SC with a large penetration depth.[24–26] In the limit $\mathbf{q}=0$, it can be shown that[24]

$$\hat{\Gamma}_\gamma(\mathbf{p},i\omega)=\Gamma_{2\gamma}(\mathbf{p},i\omega)\tau_2+\Gamma_{3\gamma}(\mathbf{p},i\omega)\tau_3. \quad (24)$$

Then Eq. (23) simplifies to $[p'=(i\epsilon',\mathbf{p}')]$

$$\Gamma_{2\gamma}(\mathbf{p},i\omega)=\frac{T}{N}\sum_{\mathbf{p}',i\epsilon'}[-\Gamma_{2\gamma}(\mathbf{p}',i\omega)A(p',i\omega) +\Gamma_{3\gamma}(\mathbf{p}',i\omega)B(p',i\omega)]\times[-D_{\mathbf{pp}'}]$$

$$\Gamma_{3\gamma}(\mathbf{p},i\omega)=\gamma_{\mathbf{p}}+\frac{T}{N}\sum_{\mathbf{p}',i\epsilon'}[\Gamma_{3\gamma}(\mathbf{p}',i\omega)C(p',i\omega) +\Gamma_{2\gamma}(\mathbf{p}',i\omega)B(p',i\omega)]\times[-D_{\mathbf{pp}'}], \quad (25)$$

where

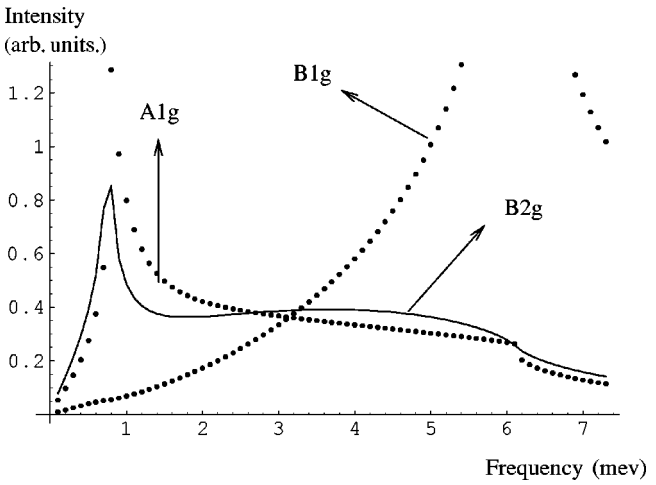

FIG. 1. Raman intensities with the bare vertex. $\Delta_g=1.72$ meV, $\Delta_s=1.34$ meV, and $T_c=15.9$ K.

$$A(p',i\omega)=\frac{i\epsilon'(i\epsilon'+i\omega)-\Delta_{\mathbf{k}'}^2-\xi_{\mathbf{k}'}^2}{[(i\epsilon')^2-E_{\mathbf{k}'}^2][(i\epsilon'+i\omega)^2-E_{\mathbf{k}'}^2]},$$

$$C(p',i\omega)=\frac{i\epsilon'(i\epsilon'+i\omega)-\Delta_{\mathbf{k}'}^2+\xi_{\mathbf{k}'}^2}{[(i\epsilon')^2-E_{\mathbf{k}'}^2][(i\epsilon'+i\omega)^2-E_{\mathbf{k}'}^2]},$$

$$B(p',i\omega)=\frac{i\Delta_{\mathbf{k}'}i\omega}{[(i\epsilon')^2-E_{\mathbf{k}'}^2][(i\epsilon'+i\omega)^2-E_{\mathbf{k}'}^2]}. \quad (26)$$

The symmetry structure of the pairing potential [Eq. (18)] and the separable kernel form of Eq. (25) imply that vertices of B_{1g} and B_{2g} symmetries are not renormalized, namely,

$$\Gamma_{2\gamma}(\mathbf{p},i\omega)=0, \quad \Gamma_{3\gamma}(\mathbf{p},i\omega)=\gamma_{\mathbf{p}} \quad \text{for} \quad B_{1g},B_{2g}. \quad (27)$$

If additional scatterings were present in particle-hole channel with B_{1g} and/or B_{2g} symmetry, the vertices for B_{1g} and B_{2g} symmetries would be renormalized.

The nontrivial correction influences only the A_{1g} vertex without the additional interactions mentioned above. The vertex correction for A_{1g} can be calculated explicitly. The details of the calculations can be found in Appendix B.

IV. RESULTS

A. Results with the bare vertex

Even though analytical solutions in closed forms are not available, the asymptotic behavior at low frequency and the peak positions of correlation functions can be understood without numerical integrations. [For a pure *d*-wave SC, the integral can be done exactly in terms of elliptic integrals.[26]] Detailed analytical calculations of low-energy behaviors of Raman susceptibilities $\pi_{\gamma\gamma}$ can be found in Appendix A. Numerical integrations are required for solutions valid over the entire frequency range. The numerical results are presented in Figs. 1 and 2. The result shown in Fig. 1, for the

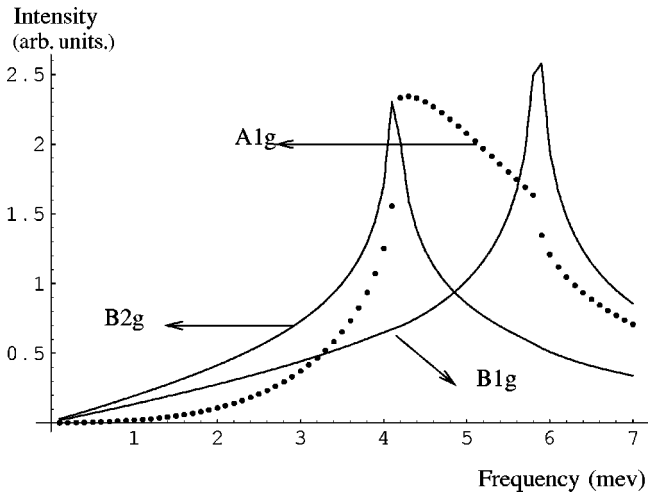

FIG. 2. Raman intensities with the bare vertex. $\Delta_g=2.5$ meV, $\Delta_s=0.43$ meV, and $T_c=14.2$ K.

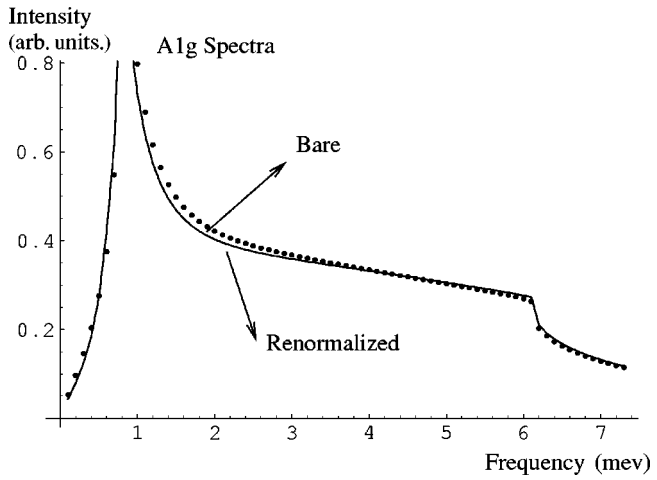

FIG. 3. Raman intensity with and without vertex correction for A_{1g} spectra. $\Delta_s=1.34$ meV, $\Delta_g=1.72$ meV, and $T_c=15.9$ K. $\lambda_s=0.13$, $\lambda_g=0.22$, and $\lambda_{sg}=0.15$. The solid line is the spectra with the vertex corretion, and the dotted line is the bare vertex spectra.

case Δ_g, is slightly larger than Δ_s, while Fig. 2 shows that the result for the case Δ_g is much larger than Δ_s.

The B_{1g} spectrum is characterized by a sharp peak at $\omega=2(\Delta_s+\Delta_g)$, and a linear frequency dependence at low-frequency. The low-frequency behavior is described by [see Eq. (A13)] $(1-\Delta_s/\Delta_g)\omega+\text{const}\times\omega^3$. Note that the slope of linear term is larger for smaller Δ_s/Δ_g.

The A_{1g} and B_{2g} spectra are characterized by a peak at $\omega=2(\Delta_g-\Delta_s)$, and a linear frequency dependence at low frequency. Without the screening correction the A_{1g} spectrum would have peaks at *both* $\omega=2(\Delta_s+\Delta_g)$ and $\omega=2(\Delta_g-\Delta_s)$ (see discussions below). The peak at $\omega=2(\Delta_s+\Delta_g)$ of the A_{1g} spectrum is canceled by the screening correction; however, a small hump feature remains at the frequency. The B_{2g} spectrum does not show a noticeable structutre at $\omega=2(\Delta_s+\Delta_g)$.

The peak positions of the above spectra are determined by the following three conditions. (A) The angular integrals Eqs. (21) and (22) can be re-expressed in terms of $z=\cos 4\phi$, then the Jacobian of the change of variable $1/\sqrt{1-z^2}$ appears in the integrand. Then large contributions to the integrals stem from the angular region where $z=\cos 4\phi\sim\pm 1$. This feature is very similar to that of a van Hove singularity. (B) Large contributions to the integrals also come from the angular region where $\omega^2-4\Delta^2(\phi)\sim 0$ [see Eq. (21)]. The frequencies which satisfy conditions (A) and (B) are $\omega=2(\Delta_g\pm\Delta_s)$, and the peaks are expected at those frequencies. (C) Conditions (A) and (B) predict peaks at *both* frequencies $\omega=2(\Delta_g+\Delta_s)$ and $2(\Delta_g-\Delta_s)$ irrespective of the scattering symmetry. The scatttering symmetry is encoded in the vertex factor $\gamma(\phi)$.

For B_{1g} symmetry, $\gamma^2(\phi)=\cos^2(2\phi)=(1+\cos 4\phi)/2$. The vertex (squared) vanishes at $\cos 4\phi=-1$, and this factor suppresses a peak that would appear at $\omega=2(\Delta_g-\Delta_s)$. [Recall that $\Delta(\phi)=\Delta_s+\Delta_g\cos 4\phi$] Therefore, for B_{1g} symmetry, only a single peak at $\omega=2(\Delta_g+\Delta_s)$ is expected, which agrees with the numerical result.

The vertex factor of B_{2g} is $\gamma^2(\phi)=\sin^2(2\phi)=(1-\cos 4\phi)/2$. Following the same arguments as the B_{1g} case, we may expect a single peak at $\omega=2(\Delta_g-\Delta_s)$, which also agrees with the numerical result. The screening corrections do not alter the above results because the corrections simply vanish for B_{1g}, B_{2g} spectra, as discussed in Sec. III A.

For the A_{1g} case, we have to take the screening correction into account. Now note that in the angular region $\cos 4\phi\sim 1$ [see Eq. (11)],

$$\pi_{\gamma_{A_1}\gamma_{A_1}}\sim\pi_{\gamma_{A_1}0}\sim\pi_{00}. \tag{28}$$

Then the contribution to the Raman susceptibility,

$$\chi_{\gamma_{A_1}\gamma_{A_1}}=\pi_{\gamma_{A_1}\gamma_{A_1}}-(\pi_{\gamma_{A_1}0})^2/\pi_{00}, \tag{29}$$

coming from the angular region $\cos 4\phi\sim 1$, becomes small due to the cancellation between the first and second terms. The above cancellations *also* occur for the contributions from the angular region $\cos 4\phi\sim -1$. Then subleading contributions determine the peaks. Numerical results show that the A_{1g} peak appears at $\omega=2(\Delta_g-\Delta_s)$.

B. Results with the renormalized vertex

As discussed in Sec. III B, the vertex correction affects only the A_{1g} spectrum. The vertex correction depends on the relative magnitude of Δ_s and Δ_g. The results are presented in Figs. 3 and 4. It turns out that the vertex correction is more important for larger Δ_g/Δ_s. In case of Fig. 3 ($\Delta_g/\Delta_s=1.28$), the vertex correction is almost negligible over the entire frequency range. On the other hand, in case of Fig. 4 ($\Delta_g/\Delta_s=5.8$), the vertex correction suppresses the peak at $\omega=2(\Delta_g-\Delta_s)$ which was present in the spectrum with the bare vertex. At low frequency, the vertex correction is negligible as in the case of Fig. 3, while at frequency higher than $2(\Delta_g+\Delta_s)$, it slightly enhances the spectrum. More discussions will follow in the next section.

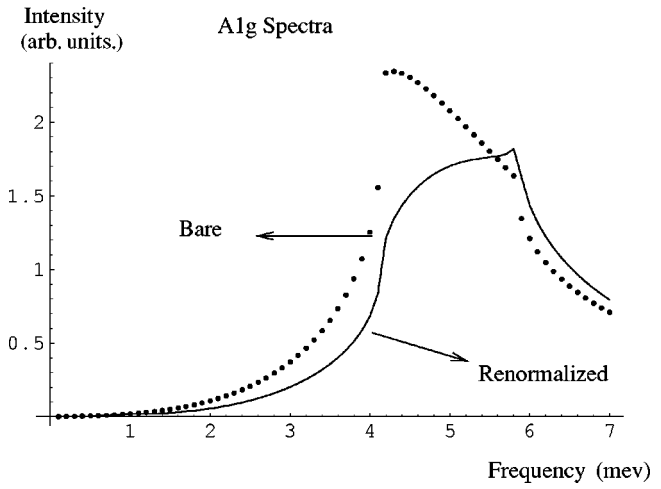

FIG. 4. Raman intensity with vertex correction for A_{1g} spectra. $\Delta_s=0.43$ meV, $\Delta_g=2.5$ meV, and $T_c=14.2$ K. $\lambda_s=0.05$, $\lambda_g=0.42$, and $\lambda_{sg}=0.06$. The solid line is the spectra with the vertex correction, and the dotted line is the bare vertex spectra.

V. DISCUSSIONS AND SUMMARY

Comparing the theoretical results, especially Fig. 2, with the experimental data [Fig. 5(b)], we find that the relative order of peak positions and the low-frequency behaviors coincide with those of experimental data. In our model, the peak of the B_{1g} spectrum is located at $\omega=2(\Delta_s+\Delta_g)$, while that of the B_{2g} and A_{1g} spectrum is located at $\omega=2(\Delta_g-\Delta_g)$. Then Δ_g and Δ_s can be extracted from the experimental data, and we obtain $\Delta_g\sim 2.5$ meV and $\Delta_s\sim 0.3$ meV. Thus it turns out that the *s*-wave component of gap is much smaller than the *g*-wave component. In fact, Fig. 2 ($\Delta_g/\Delta_s=5.8$) compares more favorably with the experimental data Fig. 5 than Fig. 1 ($\Delta_g/\Delta_s=1.28$).

We have to note that the linear frequency dependence B_{1g} spectrum at low frequency observed in the Raman experiment rules out the pure *d*-wave scenario, which predicts an ω^3 dependence (see Appendix A). The low-frequency behaviors are robust againt the effect of vertex correction and provide an unambiguous evidence for the $s+g$-wave scenario.

But the theoretical results pose some drawbacks. Most significantly, the shape of B_{1g} peak looks very different from the experimental one. Theoretical results predict a strong *sharp* peak at $\omega=2(\Delta_g+\Delta_s)$. Experimentally, the B_{1g} peak is very broad and weak compared to the A_{1g} and B_{2g} peaks.

However, there exist some caveats in comparing the theoretical results directly with the experimental data. Recall that we have included only the pairing interaction in the particle-hole channel in computing the vertex correction. Owing to the specific symmetry of the pairing interaction, the B_{1g} and B_{2g} channels were immune to the vertex correction. In general, we may well include interactions in B_{1g} and B_{2g} symmetries in the particle-hole channel which are compatible with tetragonal symmetries such as $V\cos 2\phi\cos 2\phi'$ and $W\sin 2\phi\sin 2\phi'$. If such interactions were present the B_{1g} and /or B_{2g} channels surely would be influenced by vertex corrections.

Regarding the discrepancies on the shape of B_{1g} peak

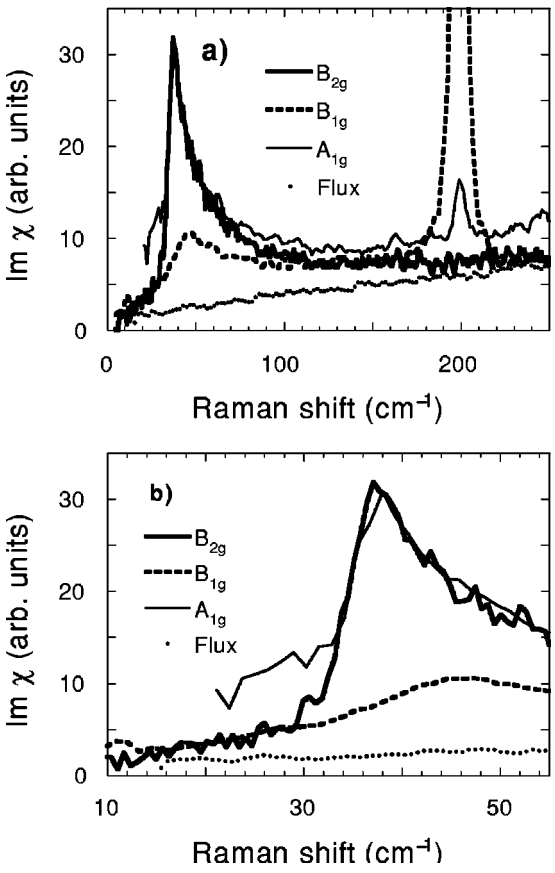

FIG. 5. Raman spectra of YNi_2B_2C with $T_c=15.3$ K from Yang *et al.*'s experiment (Ref. 23). The strong peak of (a) near 200 cm^{-1} is due to the B_{1g} phonon.

structure between the theory and the experiment, we presume that there exists a very strong inelastic scattering acting in the B_{1g} channel which suppresses and broadens the B_{1g} peak. The introduction of inelastic scattering acting on this B_{1g} channel would not modify the low-frequency behaviors, since it is mostly dictated by the symmetry of superconducting order parameter.

Borrowing the arguments in Sec. IV A, we may expect that the effect of inelastic scattering on the B_{1g} channel would be strongest near $\omega=2(\Delta_g+\Delta_s)$. Then the weak peak structure at $\omega=2(\Delta_g+\Delta_s)$ of *renormalized* A_{1g} spectraum (see Fig. 4) would be suppressed, and a peak would show up again at $\omega=2(\Delta_g-\Delta_s)$, in agreement with the experiment.

The physical origin of the hypothetical inelastic scattering acting in B_{1g} channel is not clear, but the Raman experiment [Fig. 5(a)] strongly suggests that the scattering between B_{1g} phonons and electrons might be a possible candidate. We also note that the inclusion of the detailed momentum anisotropy of SG compatible with the tetragonal symmetry would give the results which will agree better with the experiments.

It should be pointed out that the peculiar natures of Raman spectra of BCSC may be understood by the collective mode scenario.[27] The nesting property of the Fermi surface[28] is likely to play an important role in the collective mode scenario.

In summary, we have studied the electronic Raman scat-

tering of borocarbide superconductors based on the weak-coupling theory with $s+g$-wave gap symmetry. The low-frequency behaviors and the relative peak positions can be naturally understood within a simple one-loop calculation. However, there are discrepancies in the detailed shape of peak structures between theoretical predictions and experimental results. The inclusion of the strong inelastic scattering between B_{1g} phonon and electron may resolve the discrepancies.

ACKNOWLEDGMENTS

We are grateful to In-Sang Yang for useful comments, and for allowing us to reproduce his data in our paper. Fruitful discussions with Hee Sang Kim and Tae Suk Kim are also acknowledged. This work was supported by the Korea Science and Engineering Foundation (KOSEF) through Grant No. 1999-2-11400-005-5, and by the Ministry of Education through Brain Korea 21 SNU-SKKU Program.

APPENDIX A: LOW-FREQUENCY BEHAVIORS OF CORRELATION FUNCTIONS

At low frequency, the angular integral of Eq. (21) is dominated by contributions from the angular region where $\Delta(\phi)\sim 0$. In this region, the gap function $\Delta(\phi)$ can be linearized with respect to the angle ϕ_0 defined by $\Delta(\phi_0)=0$.

Let us first consider a pure d-wave case $\Delta(\phi)=\Delta_d\cos 2\phi$. If we take into account the contributions from the first quadrant only, the gap function vanishes at $\phi=\pi/4$. Writing $\phi=\pi/4+x$, $|x|\ll 1$, the integral of Eq. (21) can be reduced to

$$-\mathrm{Im}\,\pi^R_{\gamma\gamma}\sim \frac{N_F}{\omega}\int_{-\omega/4\Delta_d}^{\omega/4\Delta_d}\frac{dx}{2\pi}\frac{\gamma^2\left(\phi=\frac{\pi}{4}+x\right)[4\Delta_d^2x^2]}{\sqrt{\omega^2-16\Delta_d^2x^2}}. \tag{A1}$$

The vertex factors become [see Eq. (11)]

$$\gamma_{A_{1g}}\left(\frac{\pi}{4}+x\right)\sim -1, \tag{A2}$$

$$\gamma_{B_{1g}}\left(\frac{\pi}{4}+x\right)\sim -2x, \tag{A3}$$

$$\gamma_{B_{2g}}\left(\frac{\pi}{4}+x\right)\sim 1. \tag{A4}$$

Using scaling $x=(\omega/4\Delta_d)y$, for $\omega\ll 2\Delta_d$ we obtain

$$-\mathrm{Im}\,\pi^{R(D)}_{A_{1g}}(\omega)\sim\omega,$$

$$-\mathrm{Im}\,\pi^{R(D)}_{B_{1g}}(\omega)\sim\omega^3,$$

$$-\mathrm{Im}\,\pi^{R(D)}_{B_{2g}}(\omega)\sim\omega, \tag{A5}$$

where the superscript (D) indicates the symmetry of superconducting order parameter. Results (A5) coincide with those obtained by Devereaux and Einzel.[26]

Next let us consider the $s+g$-wave case $\Delta(\phi)=\Delta_s+\Delta_g\cos 4\phi$. Upon linearization, one can write

$$\Delta(\phi=\phi_0+x)\sim -ax,\quad a=4\Delta_g\sin 4\phi_0, \tag{A6}$$

where the angle ϕ_0 is defined by the relation

$$\Delta_s+\Delta_g\cos 4\phi_0=0,\quad \Delta_s,\Delta_g>0. \tag{A7}$$

Then the angular integral can be expressed as

$$-\mathrm{Im}\,\pi^R_{\gamma\gamma}\sim \frac{N_F}{\omega}\int_{-\omega/2a}^{\omega/2a}\frac{dx}{2\pi}\frac{\gamma^2(\phi=\phi_0+x)[a^2x^2]}{\sqrt{\omega^2-4a^2x^2}}. \tag{A8}$$

The vertex factors become

$$\gamma^2_{A_{1g}}(\phi_0+x)\sim\cos^2 4\phi_0=(\Delta_s/\Delta_g)^2, \tag{A9}$$

$$\gamma^2_{B_{1g}}(\phi_0+x)\sim\frac{1-\Delta_s/\Delta_g}{2}-[2\sin 4\phi_0]x-[4\cos 4\phi_0]x^2, \tag{A10}$$

$$\gamma^2_{B_{2g}}(\phi_0+x)\sim\frac{1+\Delta_s/\Delta_g}{2}. \tag{A11}$$

In Eq. (A10) the second term is odd in x; thus it gives a vanishing result upon integration. The first and third terms of Eq. (A10) dominate the low-energy behavior. Carrying out the integrals by rescaling as in the d-wave case, we obtain

$$-\mathrm{Im}\,\pi^{R(SG)}_{A_{1g}}(\omega)\sim\gamma^2_{A_1}(\Delta_s/\Delta_g)^2\omega, \tag{A12}$$

$$-\mathrm{Im}\,\pi^{R(SG)}_{B_{1g}}(\omega)\sim\gamma^2_{B_1}\left[\frac{1-\Delta_s/\Delta_g}{2}\right]\omega+\mathrm{const}\,\omega^3, \tag{A13}$$

$$-\mathrm{Im}\,\pi^{R(SG)}_{B_{2g}}(\omega)\sim\gamma^2_{B_2}\left[\frac{1+\Delta_s/\Delta_g}{2}\right]\omega, \tag{A14}$$

where the superscript (SG) indicates the symmetry of order parameter. The coefficients of vertex factors $\gamma^2_{A_1}$, $\gamma^2_{B_1}$, and $\gamma^2_{B_2}$ are reinstated for clarity. The above results differ from the pure d-wave case by the ω-linear component of the B_{1g} spectra. We also note the dependence on the gap ratio $0\leqslant\Delta_s/\Delta_g\leqslant 1$. For the small gap ratio, the ω-linear component of the A_{1g} spectra is suppressed, while that of the B_{1g} spectra is enhanced. This agrees well with the numerical result. (See Figs. 1 and 2.)

APPENDIX B: CALCULATION OF VERTEX CORRECTION

First write

$$\Gamma_{2,3}(i\omega,\mathbf{p})=\Gamma^s_{2,3}(i\omega)+\Gamma^g_{2,3}(i\omega)\cos 4\phi. \tag{B1}$$

Define two-component column vectors

$$\Gamma_2(i\omega)=\begin{pmatrix}\Gamma_2^s(i\omega)\\ \Gamma_2^g(i\omega)\end{pmatrix},\quad \Gamma_3(i\omega)=\begin{pmatrix}\Gamma_3^s(i\omega)\\ \Gamma_3^g(i\omega)\end{pmatrix}. \tag{B2}$$

Then the integral equation for the vertex correction [Eq. (25)] can be recast in a matrix form

$$\begin{bmatrix} I_2+A & -B \\ -B & I_2-C\end{bmatrix}\begin{bmatrix}\Gamma_2\\ \Gamma_3\end{bmatrix}=\begin{bmatrix}0\\ \tilde{\gamma}\end{bmatrix}, \tag{B3}$$

where I_2 is the 2×2 identity matrix, and A, B, and C are 2×2 matrices to be defined below. $\tilde{\gamma}$ is a two-component column vector defined by

$$\tilde{\gamma}=\begin{bmatrix}1\\0\end{bmatrix}\quad \text{for}\quad \gamma=1,$$

$$\tilde{\gamma}=\begin{bmatrix}0\\1\end{bmatrix}\quad \text{for}\quad \gamma=\cos 4\phi. \tag{B4}$$

The matrix equation (B3) can be solved, yielding the desired solutions:

$$\Gamma_{2\gamma}=[(I_2-C)B^{-1}(I_2+A)-B]^{-1}\tilde{\gamma},$$

$$\Gamma_{3\gamma}=[(I_2-C)-B(I_2+A)^{-1}B]^{-1}\tilde{\gamma}. \tag{B5}$$

The 2×2 matrices A, B, and C are defined as follows:

$$A=\begin{pmatrix}a_1 & a_2\\ a_3 & a_4\end{pmatrix},\quad B=\begin{pmatrix}b_1 & b_2\\ b_3 & b_4\end{pmatrix},\quad C=\begin{pmatrix}c_1 & c_2\\ c_3 & c_4\end{pmatrix}. \tag{B6}$$

The matrix elements are given by $[p=(i\epsilon,\mathbf{p})]$

$$a_1(i\omega)=\frac{T}{N}\sum_{i\epsilon,\mathbf{p}} I_s(\phi)A(p,i\omega),$$

$$a_2(i\omega)=\frac{T}{N}\sum_{i\epsilon,\mathbf{p}} I_s(\phi)(\cos 4\phi)A(p,i\omega),$$

$$a_3(i\omega)=\frac{T}{N}\sum_{i\epsilon,\mathbf{p}} I_g(\phi)A(p,i\omega),$$

$$a_4(i\omega)=\frac{T}{N}\sum_{i\epsilon,\mathbf{p}} I_g(\phi)(\cos 4\phi)A(p,i\omega),$$

$$b_1(i\omega)=\frac{T}{N}\sum_{i\epsilon,\mathbf{p}} I_s(\phi)B(p,i\omega),$$

$$b_2(i\omega)=\frac{T}{N}\sum_{i\epsilon,\mathbf{p}} I_s(\phi)(\cos 4\phi)B(p,i\omega),$$

$$b_3(i\omega)=\frac{T}{N}\sum_{i\epsilon,\mathbf{p}} I_g(\phi)B(p,i\omega),$$

$$b_4(i\omega)=\frac{T}{N}\sum_{i\epsilon,\mathbf{p}} I_g(\phi)(\cos 4\phi)B(p,i\omega),$$

$$c_1(i\omega)=\frac{T}{N}\sum_{i\epsilon,\mathbf{p}} I_s(\phi)C(p,i\omega),$$

$$c_2(i\omega)=\frac{T}{N}\sum_{i\epsilon,\mathbf{p}} I_s(\phi)(\cos 4\phi)C(p,i\omega),$$

$$c_3(i\omega)=\frac{T}{N}\sum_{i\epsilon,\mathbf{p}} I_g(\phi)C(p,i\omega),$$

$$c_4(i\omega)=\frac{T}{N}\sum_{i\epsilon,\mathbf{p}} I_g(\phi)(\cos 4\phi)C(p,i\omega), \tag{B7}$$

where

$$I_s(\phi)=\lambda_s+\lambda_{sg}\cos 4\phi,\quad I_g(\phi)=\lambda_g\cos 4\phi+\lambda_{sg},$$

$$\lambda_s=-N_F D_s,\quad \lambda_g=-N_F D_g,\quad \lambda_{sg}=-N_F D_{sg}. \tag{B8}$$

The vertex correction [Eq. (B5)] together with Eq. (B1) should be substituted into the integral equation (15). Note that the solutions Eq. (B5) depend only on the external frequency $i\omega$, so that just an analytical continuation $i\omega\rightarrow\omega+i\delta$ without additional integrations is sufficient to obtain the final answer.

APPENDIX C: CHOICE OF COUPLING CONSTANTS

The gap equation Eq. (17) can be written as a set of coupled equations [notations are defined in Eq. (B8)].

$$\Delta_s=\Delta_s(\lambda_s I_0+\lambda_{sg}I_1)+\Delta_g(\lambda_s+\lambda_{sg}I_2),$$

$$\Delta_g=\Delta_s(\lambda_g I_1+\lambda_{sg}I_0)+\Delta_g(\lambda_g I_2+\lambda_{sg}I_1),$$

$$I_n=\int_0^{\omega_c} d\xi_{\mathbf{p}}\int_0^{\pi}\frac{dx}{\pi}(\cos x)^n\frac{E_{\mathbf{p}}/2T}{E_{\mathbf{p}}}. \tag{C1}$$

Solving Eq. (C1) at $T=T_c$, we obtain a relation between T_c and coupling constants.

$$\ln\left[1.135\frac{\omega_c}{T_c}\right]=\frac{\left(\frac{\lambda_g}{2}+\lambda_s\right)-\left[\left(\frac{\lambda_g}{2}-\lambda_s\right)^2+2\lambda_{sg}^2\right]^{1/2}}{\lambda_s\lambda_g-\lambda_{sg}^2}. \tag{C2}$$

For a pure g-wave case, the well-known result $T_c=1.135\times\omega_c e^{-2/\lambda_g}$ is reproduced. Fixing the cutoff $\omega_c=100$ meV, we have chosen the following two sets of the coupling constants by solving Eqs. (C1) and (C2).

$$(\mathrm{I})\lambda_s=0.13,\quad \lambda_g=0.22,\quad \lambda_{sg}=0.15,$$

$$\Delta_s=1.34\ \mathrm{meV},\quad \Delta_g=1.72\ \mathrm{meV},\quad T_c=15.9\ \mathrm{K}; \tag{C3}$$

$$(\mathrm{II})\lambda_s=0.05,\quad \lambda_g=0.42,\quad \lambda_{sg}=0.06,$$

$$\Delta_s=0.43\ \mathrm{meV},\quad \Delta_g=2.5\ \mathrm{meV},\quad T_c=14.2\ \mathrm{K}. \tag{C4}$$

*Electronic address: hyunlee@phys1.skku.ac.kr

[1] S. L. Cooper, *Handbook on the Physics and Chemistry of Rare Earths* (Elsevier Science, 2001), Vol. 31, p. 505.

[2] R. Nagarajan, C. Mazumdar, Z. Hossain, S.K. Dhar, K.V. Gopalakrishnan, L.C. Gupta, C. Godart, B.D. Padalia, and R. Vijayaraghahan, Phys. Rev. Lett. **72**, 274 (1994); R.J. Cava, H. Takagi, H.W. Zandbergen, J.J. Krajewski, W.F. Pock, Jr., T. Siegrist, B. Battogg, R.B. van Dover, R.J. Felder, K. Mizuhashi, J.O. Lee, H. Eisaki, and S. Uchida, Nature (London) **367**, 252 (1994).

[3] See, for example, K. Ishida, H. Mukuda, Y. Kitaoka, K. Asayama, Z.Q. Mao, Y. Mori, and Y. Maeno, Nature (London) **396**, 658 (1998).

[4] J. Annett, N. Goldenfeld, and A. J. Leggett, in *Physical Properties of High Temperature Superconductors*, edited by D. M. Ginsberg (World Scientific, Singapore, 1996), Vol. V, p. 375.

[5] W.E. Pickett and D.J. Singh, Phys. Rev. Lett. **72**, 3702 (1994).

[6] J.I. Lee, T.S. Zhao, I.G. Kim, B.I. Min, and S.J. Youn, Phys. Rev. B **50**, 4030 (1994).

[7] S.A. Carter, B. Batlogg, R. Cava, J.J. Krajewski, and W.F. Peck, Jr., Phys. Rev. B **50**, 4216 (1994).

[8] G.-Q. Zheng, Y. Wade, K. Hashimoto, Y. Kitaoka, K. Asayama, H. Takeya, and K. Kadowaki, J. Phys. Chem. Solids **59**, 2169 (1998).

[9] M. Sigrist and K. Ueda, Rev. Mod. Phys. **63**, 239 (1991).

[10] M. Nohara, M. Isshik, H. Takagi, and R.J. Cava, J. Phys. Soc. Jpn. **66**, 1888 (1997).

[11] M. Nohara, M. Isshiki, F. Sakai, and H. Takagi, J. Phys. Soc. Jpn. **68**, 1078 (1999).

[12] G.E. Volovik, Pis'ma Zh. Éksp. Teor. Fiz. **58**, 457 (1993) [JETP Lett. **58**, 472 (1993)].

[13] V. Metlushko, U. Welp, A. Koshelev, I. Aranson, and G.W. Crabtree, Phys. Rev. Lett. **79**, 1738 (1997).

[14] G. Wang and K. Maki, Phys. Rev. B **58**, 6493 (1998).

[15] T. Yokoya, T. Kiss, T. Watanabe, S. Shin, M. Nohara, H. Takagi, and T. Oguchi, Phys. Rev. Lett. **85**, 4952 (2000).

[16] E. Boaknin, R.W. Hill, C. Proust, C. Lupien, L. Taillefer, and P.C. Canfield, cond-mat/0108409 (unpublished).

[17] C. Caroli, P.G. de Gennes, and J. Matricon, Phys. Lett. **9**, 307 (1964).

[18] M. Nohara, M. Isshiki, F. Sakai, and H. Takagi, Physica C **341-348**, 2177 (2000).

[19] L.S. Borkowski and P.K. Hirschfeld, Phys. Rev. B **49**, 15404 (1994); R. Fehrenbacher and M.R. Norman, *ibid.* **50**, 3495 (1994).

[20] P.W. Anderson, J. Phys. Chem. Solids **11**, 26 (1959).

[21] A.I. Larkin, Pis'ma Zh. Éksp. Teor. Fiz. **2**, 205 (1965) [JETP Lett. **2**, 130 (1965)].

[22] K. Maki, P. Thalmeier, and H. Won, cond-mat/0110591 (unpublished).

[23] In-Sang Yang, M.V. Klein, S.L. Cooper, P.C. Canfield, B.K. Cho, and Sung-Ik Lee, Phys. Rev. B **62**, 1291 (2000).

[24] M.V. Klein and S.B. Dieker, Phys. Rev. B **29**, 4976 (1984).

[25] H. Monien and A. Zawadowski, Phys. Rev. B **41**, 8798 (1990).

[26] T.P. Devereaux and E. Einzel, Phys. Rev. B **51**, 16 336 (1995); **54**, 15 547(E) (1995).

[27] H. Ghosh and M. Sardar, Physica C **288**, 121 (1997); **246**, 355 (1995).

[28] H. Kawano, H. Yoshizawa, H. Takeya, and K. Kadowaki, Phys. Rev. Lett. **77**, 4628 (1996).